www.nature.com/scientificreports

scientific reports

OPEN

Anisotropy of magnetic damping in Ta/CoFeB/MgO heterostructures

Bivas Rana[1,2]✉ & YoshiChika Otani[2,3]

Magnetic damping controls the performance and operational speed of many spintronics devices. Being a tensor quantity, the damping in magnetic thin films often shows anisotropic behavior with the magnetization orientation. Here, we have studied the anisotropy of damping in Ta/CoFeB/MgO heterostructures, deposited on thermally oxidized Si substrates, as a function of the orientation of magnetization. By performing ferromagnetic resonance (FMR) measurements based on spin pumping and inverse spin Hall effect (ISHE), we extract the damping parameter in those films and find that the anisotropy of damping contains four-fold and two-fold anisotropy terms. We infer that four-fold anisotropy originates from two-magnon scattering (TMS). By studying reference Ta/CoFeB/MgO films, deposited on $LiNbO_3$ substrates, we find that the two-fold anisotropy is correlated with in-plane magnetic anisotropy (IMA) of the films, suggesting its origin as the anisotropy in bulk spin–orbit coupling (SOC) of CoFeB film. We conclude that when IMA is very small, it's correlation with two-fold anisotropy cannot be experimentally identified. However, as IMA increases, it starts to show a correlation with two-fold anisotropy in damping. These results will be beneficial for designing future spintronics devices.

Magnetic damping, one of the critical parameters of magnetic materials, governs the performance and operational speed of many proposed spintronics devices. It decides how fast the energy of the spin system sustaining the precessional magnetization motion dissipates into the nonmagnetic systems such as lattice, substrate, the environment through the interactions like magnon-magnon, magnon-electron, magnon-phonon and so on[1]. Initially, damping was thought to be a scalar quantity, i.e., isotropic in a magnetic material. Later, many theoretical studies[2–4] predicted and experimental studies[5–9] demonstrated that the damping is a tensor quantity and anisotropic. This essentially means that the damping depends on the magnetization orientation (known as *orientational anisotropy*). The anisotropy of damping becomes more prominent in magnetic materials with higher spin–orbit coupling (SOC) strength, which may originate from bulk and/or interfaces of magnetic thin film heterostructures.

Damping in magnetic thin films has many intrinsic and extrinsic sources. Using theoretical models[10–13] and experimental reports[14,15], the intrinsic component of damping α_{int} can be written as $\alpha_{int} = n(E_F)\delta^2\tau^{-1}$, where $n(E_F)$ is the density of states (DOS) at the Fermi level, δ is the SOC strength and τ is the electron scattering time. It turns out that the intrinsic damping of a magnetic material can be optimized by adjusting these three parameters, i.e., by engineering electronic band structure at the Fermi level, as demonstrated by Schoen et al.[16]. The damping can show anisotropic behavior in the presence of anisotropic DOS at the Fermi level, as the shape of the Fermi surface depends upon the direction of magnetization because of SOC[8]. Likewise, anisotropic SOC strength may also generate anisotropy in damping[9]. However, the presence of sufficiently high scattering rates often smear the anisotropic damping behavior in many magnetic systems. Other intrinsic source of damping, such as magnon-phonon coupling[17] (primarily observed in magnetostrictive films like Ni) do not impose anisotropy. In magnetic thin film heterostructures, the spin pumping (SP)[18–21] into adjacent heavy metals with high SOC strength and spin memory loss (SML)[22,23] at the interfaces are identified as additional sources of damping. However, both sources do not impose any anisotropy in damping. Apart from the above-mentioned intrinsic sources, there are several extrinsic sources of damping, such as Eddy current[24,25] (observed in relatively thicker magnetic films) and two-magnon scattering (TMS). The Eddy current damping is not responsible for anisotropic damping behavior. TMS is observed because the uniform magnons (wavevector $k \sim 0$) are scattered from inhomogeneities or imperfections present at the interfaces and converted into degenerate nonuniform magnons ($k \neq 0$)[26–28]. The TMS, observed for in-plane magnetization orientation, induces strong anisotropy in the damping, especially for ultrathin magnetic films, where interfacial effects become prominent[26,27,29]. Recently, Zhu et al. showed that the TMS in heavy-metal (HM)/ferromagnet/oxide heterostructures arises primarily at the HM/ferromagnet interface. In contrast, TMS

[1]Institute of Spintronics and Quantum Information, Faculty of Physics, Adam Mickiewicz University in Poznań, Uniwersytetu Poznanskiego 2, 61-614 Poznan, Poland. [2]Center for Emergent Matter Science, RIKEN, 2-1 Hirosawa, Wako 351-0198, Japan. [3]Institute for Solid State Physics, University of Tokyo, Kashiwa, Chiba 277-8581, Japan. ✉email: bivran@amu.edu.pl; bivasranaiitd@gmail.com

at the ferromagnet/oxide interface is relatively weak. The TMS increases with the SOC strength and magnetic inhomogeneities at HM/ferromagnet interface[28]. Overall, the anisotropy in damping arises due to magnetization orientation-dependent anisotropy in DOS and SOC, and the anisotropic nature of TMS. Intrinsic damping is known as viscous damping, which means the resonance linewidth increases linearly with the resonance frequency. TMS, on the other hand, shows a complex nonlinear dependence on resonance frequency[30–32]. However, TMS was also found to show a linear dependence on frequency[30,33,34]. It is especially observed when the resonance linewidth is measured for a short range of frequency, or the low frequency phenomena (e.g. inhomogeneous line broadening) overshadow the nonlinear behavior, and/or contribution from TMS is relatively weaker than others. This makes it quite challenging to isolate intrinsic damping from the damping caused by TMS.

Recently the studies of various physical phenomena originated at the surfaces/interfaces of magnetic thin films[35–40] owing to interfacial SOC are in high demand because of their possible potential applications in future spintronics devices. Naturally, investigation of the damping constants of magnetic thin films and their heterostructures, where interfaces play a key role on the damping constant, has also gained momentum in recent years. Efforts have been made to control the damping constant by thickness variation[41–43], material engineering[16], electric field[44,45]. Consecutively, orientational anisotropy also shows a route towards the control of damping just by changing the orientation of the magnetic field without replacing the magnetic film, which is quite appealing from the application point of view. In the current study, we report the anisotropy of damping in Ta/CoFeB/MgO heterostructures deposited on thermally oxidized Si and $LiNbO_3$ substrates. We find that the anisotropy of damping is composed of four-fold and two-fold anisotropy terms. We infer that the four-fold anisotropy originates from TMS. On the other hand, the two-fold anisotropy that correlates with the in-plane magnetic anisotropy (IMA) of the films, originates from bulk SOC of CoFeB film.

Results

Device structure and measurement principle. The sample fabrication and measurement principle are discussed in detail in the "Methods" section and can be found in references[45,46]. The devices for this study were fabricated from the multilayer stacks Ta(10)/$Co_{20}Fe_{60}B_{20}$ (t = 1.6, 1.8, 2.0, 2.2)/MgO(2)/Al_2O_3(10) deposited on thermally oxidized Si[001] substrates, and Ta(10)/$Co_{20}Fe_{60}B_{20}$ (t = 2.0)/MgO(2)/Al_2O_3(10) deposited on Y-cut $LiNbO_3$ substrates[47]. The numbers in the parentheses indicate the thicknesses of the corresponding layers. For simplicity, the films are denoted as substrate/Ta/CoFeB(t)/MgO in this article. As described in the "Methods" section, a microwave current (I_{rf}) from a signal generator, passing through the antenna, excites FMR in rectangular-shaped CoFeB films (Fig. 1a). The resonance signals are detected by measuring potential drop across the rectangular devices originated from SP and inverse spin Hall effect (ISHE).

Figure 1b represents a measured FMR signal (solid dots) from Si/SiO_2/Ta/CoFeB(2.2)/MgO film. The microwave power for all the measurements were set well below the nonlinear regime (see Supplementary Fig. S1). The values of resonance field (H_0) and resonance linewidth are determined by fitting the FMR signals to the following expression[48–50]:

$$V_{\mathrm{ISHE}} = V_0 + \frac{V_s}{1 + (H - H_0)^2/\sigma^2} + \frac{V_a(H - H_0)/\sigma}{1 + (H - H_0)^2/\sigma^2} \tag{1}$$

Here, V_0 is the background of V_{ISHE}, V_s & V_a are the weights of the symmetric Lorentzian and dispersive functions, respectively, and σ is the half-width at half maximum (HWHM) of the FMR spectrum. The almost perfect symmetric Lorentzian shape of the ISHE signal ensures that the FMR is predominantly excited by the out-of-plane component of the microwave Oersted field[18].

Out-of-plane and in-plane magnetic anisotropies of the films. The out-of-plane and in-plane magnetic anisotropies of the studied films were characterized by measuring resonance signals for different orientations (θ) of the in-plane bias magnetic field, i.e., magnetization. In all the measurements the applied bias magnetic field was set much larger than the IMA field, which rules out the increment of FMR linewidth as a consequence of field dragging effect. The resonance field ($\mu_0 H_0$) corresponding to each FMR spectra is extracted by fitting with Eq. (1) and plotted as a function of θ (see Fig. 2). The $\mu_0 H_0$ versus θ data points are subsequently fitted to the following analytical equation[51]:

$$\begin{aligned} H_0 = {} & -H_k + \frac{3}{2} H_k sin^2(\theta + \beta) - \frac{(M_s - H_p)}{2} \\ & + \frac{1}{2}\left[H_k^2 sin^4(\theta + \beta) + (M_s - H_p)^2 + 2(M_s - H_p) H_k sin^2(\theta + \beta) + 4\left(\frac{f}{\mu_0 \gamma}\right)^2\right]^{\frac{1}{2}} \end{aligned} \tag{2}$$

Here, γ is the gyromagnetic ratio, μ_0 is the permeability of free space, f is the microwave frequency, i.e., FMR frequency, H_k stands for the in-plane magnetic anisotropy (IMA) field with β being the direction of the IMA axis with respect to the long axes of the rectangular CoFeB structures, M_s is the saturation magnetization, and H_p stands for the perpendicular magnetic anisotropy (PMA) field. Figure 2 shows the polar plot of $\mu_0 H_0$ (solid points) as a function of θ for Si/SiO_2/Ta/CoFeB(t)/MgO films. The angular variation of $\mu_0 H_0$ are well fitted with Eq. (2) as shown by the solid curves. It should be noted here that different microwave frequencies were used for different films so that the resonance fields for all the films fall in the range between 125 and 150 mT, close to the half of the maximum external magnetic field used for the measurements. This helps us to fit all the obtained FMR data very nicely with the Eq. (1). However, choosing different frequency for same sample should not affect

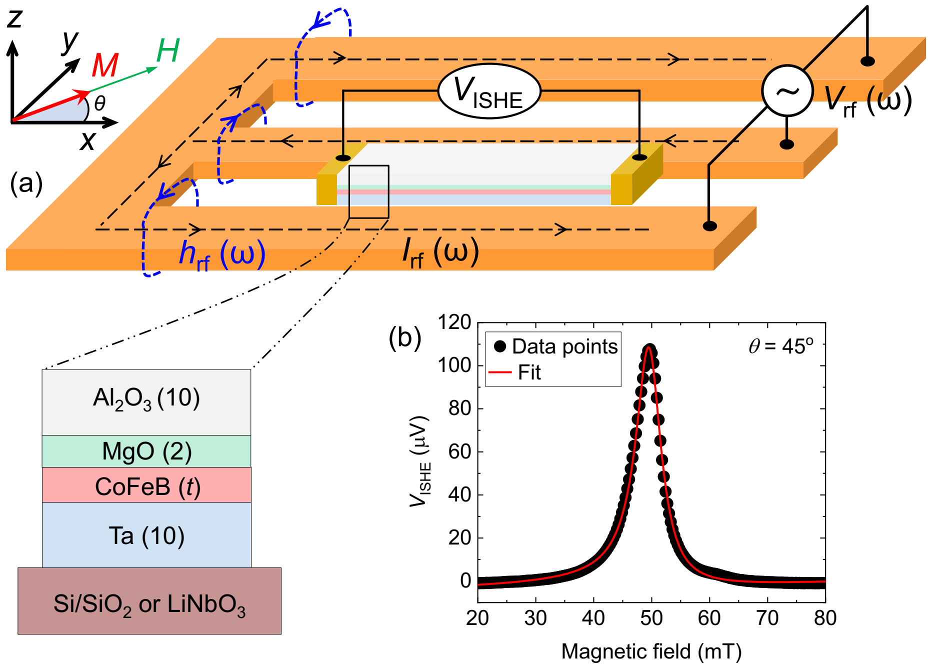

Figure 1. Device structure and measurement principle. (**a**) The schematic illustration represents the ferromagnetic resonance (FMR) measurement setup. A radio frequency current I_{rf} (ω) passes through a coplanar waveguide surrounding the rectangular-shaped multilayer film. The Oersted field h_{rf} (ω), induced by I_{rf} (ω), excites the FMR in CoFeB films at resonance condition given by Eq. (2). The magnetic field H is applied in the film plane at an angle (θ) to the long axis of the film. The FMR signals are detected by measuring potential drop (V_{ISHE}) across the rectangular multilayer film. Inset shows the cross-section of the multilayer film. (**b**) A typical ISHE signal measured from Si/SiO_2/Ta/CoFeB(2.2)/MgO film at 5 GHz microwave frequency and 18 dBm (i.e., 63 mW) microwave power is presented. The solid line represents the fit to Eq. (1).

the extracted values of the PMA and IMA fields. The extracted values of PMA fields $\mu_0 H_p$ are 0.996, 1.151, 1.252, 1.452 T, and IMA fields $\mu_0 H_k$ are 0.98 ± 0.06, 0.52 ± 0.06, 0.48 ± 0.04, 0.43 ± 0.05 mT for t = 2.2, 2.0, 1.8, 1.6 nm, respectively. Here saturation magnetization $\mu_0 M_s$ for all the films are considered to be 1.5 T[50]. Figure 3a shows the plot of $\mu_0 H_p$ as a function of t, which clarifies that PMA has purely interfacial origin as $\mu_0 H_p$ is inversely proportional to t (not shown). The IMA axes in the films with t = 2.2, 2.0, 1.8, and 1.6 nm, respectively, orient along 110°, 116°, 123°, and 148° to the long axes of the rectangular structures. It should be noted here that the extracted values of IMA fields (we say apparent IMA fields) are actually the resultant of the shape anisotropy of rectangular CoFeB films with dimension 200 × 12 μm^2 and the actual IMA introduced by crystal structure. The shape anisotropy of all the rectangular CoFeB films are about 0.76 mT. By performing simple vector alzebra the actual IMA field values come out to be 1.01 ± 0.06, 0.71 ± 0.06, 0.64 ± 0.04, 0.46 ± 0.04 mT and IMA axes are oriented along 65°, 41°, 40°, and 62° to the long axes of the rectangular structures for t = 2.2, 2.0, 1.8, 1.6 nm, respectively. Figure 3b shows the plot of actual $\mu_0 H_k$ as a function of t. The $\mu_0 H_k$ increases with the increase of t, which means IMA may primarily have bulk origin. It is important to note here that the interfacial origin of IMA was reported in the previous works[51,52]. The strain developed inside CoFeB films during deposition and annealing could be one of the possible reasons behind IMA. However, more studies are required to unveil the origin. In our films, the IMA appears by annealing without an in-plane magnetic field, resulting in a different in-plane anisotropy axis in the films. Interestingly, the values of induced IMA are within 0.1% of the PMA.

Anisotropy of damping. The total linewidth (σ) of a FMR spectra can be simply expressed as[16]:

$$\sigma = \sigma_0 + \frac{2\pi\alpha}{\gamma} f_{\mathrm{FMR}} \tag{3}$$

Here, σ_0 is the frequency independent linewidth, originates from the inhomogeneous distribution of magnetic properties (such as PMA, IMA) of the ferromagnetic (FM) films, especially, in ultrathin films. The second term, which is proportional to the resonance frequency f, originates from the relaxation of spin angular momentum through: (1) intrinsic bulk SOC of FM film itself; (2) SP into the adjacent heavy metallic layer possessing high SOC strength; (3) interfacial SOC and interfacial SML. Hence to evaluate viscous damping α, the extracted values of HWHM of FMR spectra are plotted as a function of f and fitted with a linear function. The values of α are then extracted from the slopes (Δ) of the linear fittings using the following expression[49]:

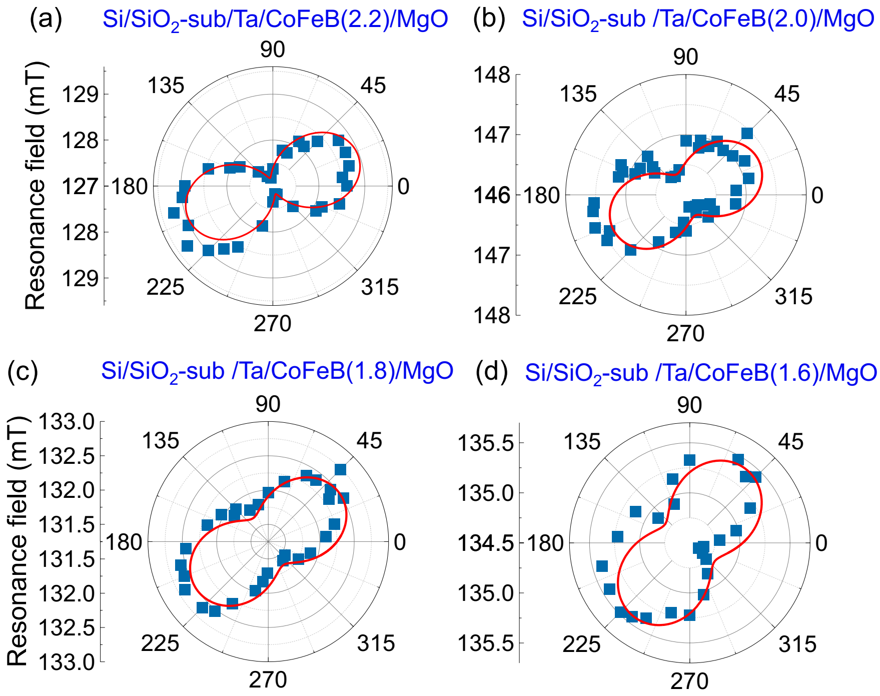

Figure 2. Resonance field versus in-plane magnetic field direction. The resonance field ($\mu_0 H_0$) versus in-plane magnetic field angle (θ) plot for Si/SiO$_2$/Ta/CoFeB(t)/MgO films with CoFeB layer thickness t = 2.2 (**a**), 2.0 (**b**), 1.8 (**c**), and 1.6 nm (**d**). The resonance fields ($\mu_0 H_0$) were measured at microwave frequencies f = 8.5, 7.8, 6.5, 4.5 GHz and microwave powers of 18, 18, 16, 14 dBm for t = 2.2, 2.0, 1.8, and 1.6 nm, respectively. The solid curves are fits to the Eq. (2).

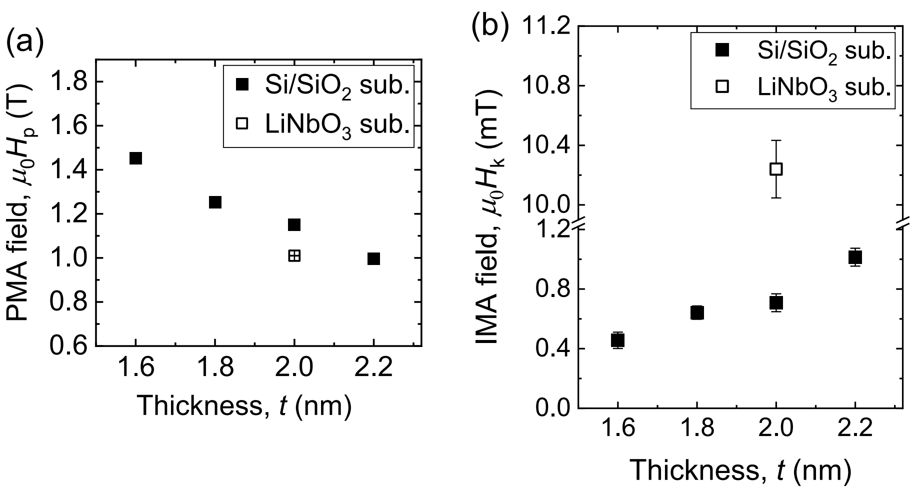

Figure 3. Anisotropy fields versus film thickness. The extracted values of PMA field ($\mu_0 H_p$) (**a**), and IMA field ($\mu_0 H_k$) (**b**) are plotted as a function of CoFeB film thickness. The error bars are included within the symbols.

$$\alpha = \frac{\gamma}{2\pi}\Delta \tag{4}$$

Figure 4a represents the plot of HWHM as a function of f for Si/SiO$_2$/Ta/CoFeB(2.2)/MgO film for 45° orientation of magnetic field, i.e., magnetization. Solid line represents linear fit. Please note that we have excluded here frequency dependent nonlinear term in the resonance linewidth [in Eq. (3)], which should be originated from TMS process. This is because all the linewidth versus frequency data show perfectly linear dependence. So, it is not really necessary to fit with nonlinear function. The reasons behind this linear behavior could be the short range of measurement frequency. To understand the angular dependent behavior of damping we plot the

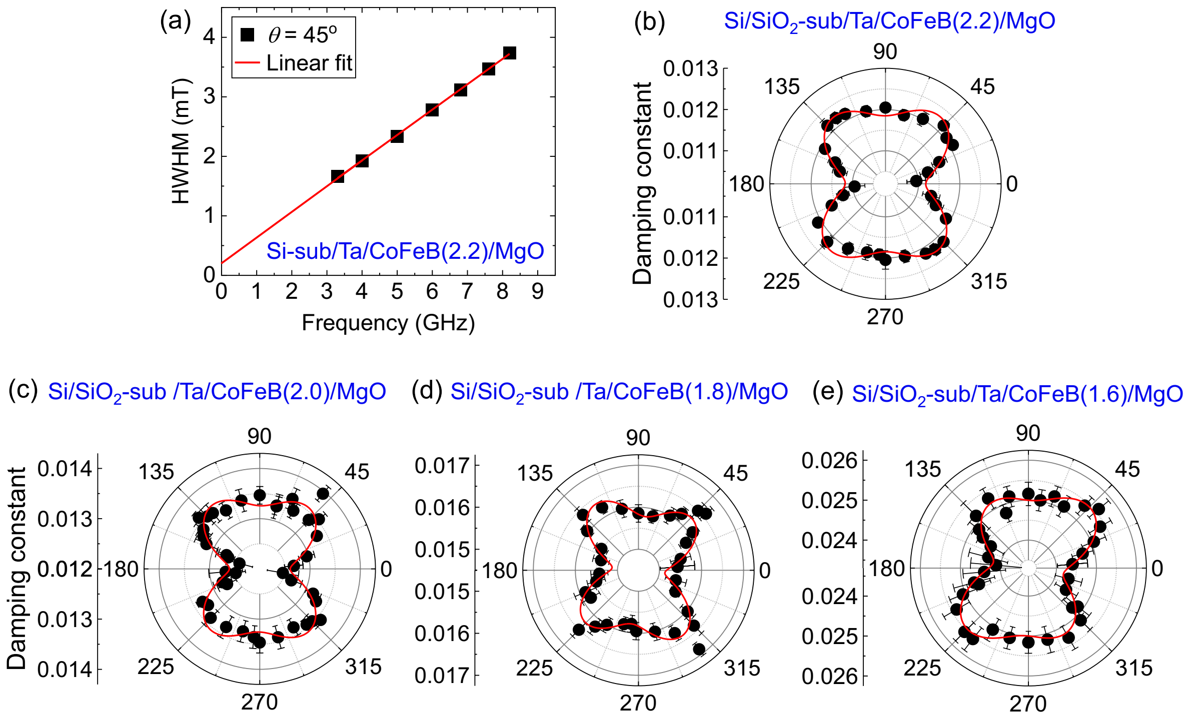

Figure 4. Angular variation of damping constant. (**a**) Resonance linewidth versus frequency plot for Si/SiO_2/Ta/CoFeB(2.2)/MgO film at 45° magnetic field orientation. Solid line represents linear fit. The extracted values of the damping constant are plotted (filled points) as a function of the in-plane orientation of the magnetic field for Si/SiO_2/Ta/CoFeB(t)/MgO films with $t = 2.2$ (**b**), 2.0 (**c**), 1.8 (**d**) and 1.6 nm (**e**). The solid curves represent the fits to Eq. (5).

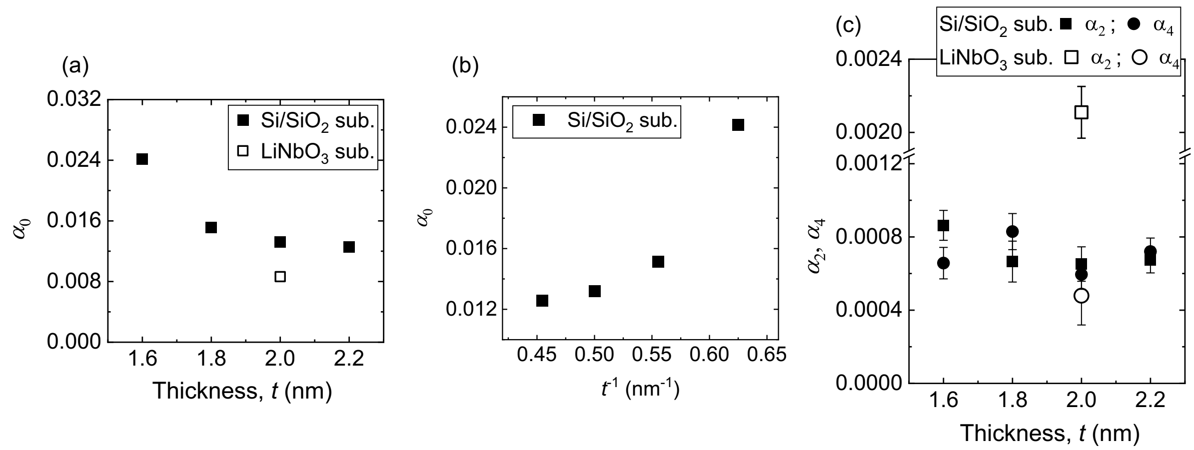

Figure 5. Damping coefficients versus film thickness. The extracted values of α_0 for Ta/CoFeB/MgO films, deposited on Si/SiO_2 and $LiNbO_3$ substrates, are plotted as a function of (**a**) CoFeB film thickness t and (**b**) t^{-1}. (**c**) Extracted values α_2, α_4 for all the Ta/CoFeB/MgO films are plotted as a function of t.

extracted values of α as a function of θ in Fig. 4b–e for Si/SiO_2/Ta/CoFeB ($t = 2.2$, 2.0, 1.8, 1.6)/MgO films. The angular variation of damping shows a four-fold anisotropy overlapped with a two-fold anisotropy. Based on previous publications[6,8,26] we assume that the observed angular behavior of α can be best fitted with the following phenomenological formula:

$$\alpha = \alpha_0 + \alpha_2 sin^2\left(\theta + \beta'\right) + \alpha_4 sin^2 2\left(\theta + \beta'\right). \tag{5}$$

Here α_0 is the θ independent isotropic component of damping; α_2, α_4 are the coefficients of two-fold and four-fold anisotropies, respectively; β' is the offset angle. Figure 4b–e show that the angular variation of α is well fitted with Eq. (5). The extracted values of the coefficients of damping are plotted as a function of t in Fig. 5. The α_0 increases monotonically with the decrease of t (see Fig. 5a). The SP and SML usually lead to inverse thickness

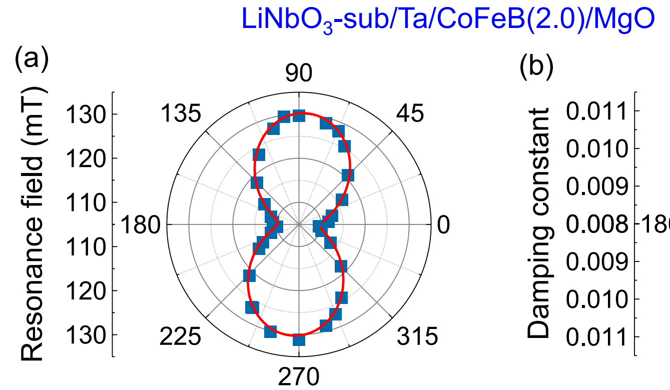

Figure 6. Angular dependence of resonance field and damping. (**a**) The resonance field ($\mu_0 H_0$) versus in-plane magnetic field angle (θ) plot for $LiNbO_3$/Ta/CoFeB(2)/MgO film. The resonance fields ($\mu_0 H_0$) were measured at 8 GHz microwave frequency and 18 dBm microwave power. The solid curve is the fit to Eq. (2). (**b**) The extracted values of damping constant are plotted (filled points) as a function of in-plane orientation (θ) of magnetic field for $LiNbO_3$/Ta/CoFeB(2)/MgO film. The solid curve is the fit to Eq. (5).

(t^{-1}) dependence of damping[22,53,54], which is not observed in our case (see Fig. 5b). This indicates that the SP and SML are not solely responsible for the observed FM layer thickness-dependent damping behavior. So, TMS must have a significant contribution to the observed damping in our films, even though FMR linewidth shows linear dependence with frequency, according to the previous reports[30,34,55]. Although resonance linewidth produced by TMS should have a complex nonlinear dependence with frequency, these articles also mentioned that the linear frequency dependence of linewidth doesn't guarantee the absence of the TMS process. It is especially true in the current study as the resonance linewidth is measured for a short range of frequency. Then it becomes quite difficult to completely isolate TMS contribution from viscous damping. Figure 5c shows that the coefficients α_2, α_4 vary randomly or, better to say, remain almost unchanged with t (solid points). The α_2, α_4 show their values up to 6% to α_0, which is relatively low compared to the previous reports[6,8,9,56]. It turns out that our experimental method can probe and quantify even the presence of tiny anisotropy in the damping.

The anisotropic natures of TMS, SOC, and DOS can explain the anisotropic behavior of damping. The previous reports demonstrated that TMS could induce four-fold anisotropy in damping for cubic crystals[26,30,34]. In HM/ferromagnet/oxide heterostructures such as Ta/CoFeB/MgO, made of ultrathin FM layer, the significant contribution of TMS comes from the HM/ferromagnet interface due to the presence of strong interfacial SOC and interfacial roughness[28]. It is argued that the TMS contribution from ferromagnet/oxide interface is relatively weaker than the HM/ferromagnet interface. We infer that the extrinsic TMS at both (Ta/CoFeB and CoFeB/MgO) interfaces is responsible for the observed four-fold anisotropy of damping (α_4) in our films. Usually, it can be expected that the lattice symmetry at the interface should replicate to the anisotropy in the damping caused by TMS. Now, all the layers in the studied films have cubic crystal structures [i.e. Ta, CoFeB, MgO have bcc, bcc and fcc crystal structures, respectively] after the annealing[57,58]. Therefore, it is quite natural that the TMS should have four-fold symmetry following the cubic symmetries at both interfaces. Another interesting point to note here that the TMS strength should show an inverse square relationship with t_{CoFeB} as discussed in the references[31,59,60]. In our case the measured range of microwave frequency is quite small and hence the linewidth versus frequency data cannot be fitted with the nonlinear function, responsible for TMS. As a result the nonlinear dependence of resonance linewidth with the frequency is overshadowed. Therefore, it is not possible for us to correctly evaluate the TMS strength. Although four-fold anisotropy in damping is solely originated from TMS, some part of the TMS induced damping may be leaked into the viscous damping (α_0). That's the reason α_0 does not also show linear relationship with $1/t_{CoFeB}$ (see Fig. 5b). For the same reason α_4, that primarily originates from TMS, does not show an inverse square relationship with t_{CoFeB}, which is very clear from Fig. 5c and Supplementary Fig. S2.

Next we would like to find out the origin of two-fold anisotropy (α_2) in damping. A correlation between α_2 and IMA is expected to be observed if α_2 originates from the anisotropies in the DOS and/or SOC in CoFeB films. However, α_2 doesn't show similar variation with t like IMA and the directions of α_2 do not coincide with the axes of IMA (i.e. $\beta^{'} \neq \beta$). In all the films, the directions of α_2 are along long axis of rectangular CoFeB film (i.e. $\beta^{'} = 0$). Therefore we cannot claim here that the anisotropies in the DOS and/or SOC in CoFeB films and its interfaces are responsible for the observed two-fold anisotropy. Hence, we studied a reference sample to investigate the origin of α_2.

Measurement of reference samples. We measured the angular-dependent behavior of damping in a reference sample: Ta/CoFeB(2)/MgO deposited on Y-cut $LiNbO_3$. By fitting the resonance field $\mu_0 H_0$ versus magnetic field angle θ to Eq. (2) (see Fig. 6a), we find that the PMA and IMA fields for this film are 1.01 T and 11 ± 0.19 mT, respectively (see Fig. 3a,b). The actual IMA field is 10.24 ± 0.19 mT and IMA appears along the x-axis. We observe a 15-fold increment in the IMA when the same film is deposited on the $LiNbO_3$ substrate compared to Si/SiO_2 substrate. Here, the $LiNbO_3$ substrate promotes the crystallization axes of the CoFeB film so that the IMA is induced along the x-axis, i.e., along the long axis of the rectangular film. A slight reduction in PMA (which has interfacial origin) indicates that the IMA may primarily have bulk origin in the deposited films on $LiNbO_3$ substrate; otherwise, IMA should have decreased like PMA. As plotted in Fig. 6b, the angular-dependent damping behavior shows the dominating two-fold orientational anisotropy along the IMA axis. The value α_2 for $LiNbO_3$/Ta/CoFeB(2)/MgO film, extracted from the fitting to Eq. (5), shows a three-fold increment compared to the α_2 for Si/SiO_2/Ta/CoFeB(2)/MgO film, suggesting a direct correlation between α_2 and IMA. Notably, the direction of α_2 is merged with the axis of IMA. Therefore, the anisotropy of SOC in CoFeB films is responsible for the observed two-fold anisotropy. Please note that IMA doesn't cause the anisotropy in damping. However, as both of them originate from the anisotropy of SOC in CoFeB films, a correlation between these parameters is observed. The reduction of α_4 for $LiNbO_3$/Ta/CoFeB(2)/MgO film compared to the α_4 for Si/SiO_2/Ta/CoFeB(2)/MgO films discards any correlation between α_4 and IMA, indicating its origin as TMS. Based on our observation, we argue that when IMA is very small (for Si/SiO_2/Ta/CoFeB(t)/MgO films), it's correlation with α_2 cannot be experimentally identified. However, as IMA increases (for $LiNbO_3$/Ta/CoFeB(2)/MgO films), it starts to show a correlation with α_2 as both originate from bulk SOC of CoFeB films.

Previous study showed that the four-fold TMS can also be originated from the crystallographic defects[61]. In that case a correlation between four-fold TMS and four-fold magnetic anisotropy should be observed. However, this is unlikely in the present study as the films do not posses four-fold magnetic anisotropy. Another study showed that the two-fold anisotropy in damping can be originated from TMS, caused by the scattering from the artificial crystal defects created by oblique incidence of target material during film deposition[62]. We also exclude this mechanism as a correlation between two-fold anisotropy in damping and IMA is observed. Moreover, our films were deposited by sputtering method.

Conclusions

In this work, we have investigated in-plane magnetization orientation-dependent anisotropy, i.e., orientational anisotropy of damping in Ta/CoFeB/MgO heterostructures deposited on thermally oxidized Si substrates. The damping constants are extracted by performing a ferromagnetic resonance (FMR) experiment excited by microwave current-induced Oersted field and detected through spin pumping (SP) and inverse spin Hall effect (ISHE) technique. The CoFeB films possess in-plane magnetic anisotropy (IMA), which increases with the film thickness suggesting its primary origin from the bulk spin–orbit coupling (SOC) of CoFeB films. The magnetization orientation-dependent damping consists of four-fold and two-fold anisotropies. We infer that the four-fold anisotropy originates from two-magnon scattering (TMS), which occurs because of the scattering of uniform magnons from inhomogeneities or imperfections at Ta/CoFeB and CoFeB/MgO interfaces to create degenerate nonuniform magnons. We do not observe any correlation between two-fold orientational anisotropy and IMA for Si/SiO_2/Ta/CoFeB/MgO films, most probably because of the small value of IMA (i.e. small anisotropy in SOC strength). However, we find a direct correlation between two-fold orientational anisotropy and IMA in reference $LiNbO_3$/Ta/CoFeB/MgO films, that contain strong IMA. This suggests that two-fold anisotropy in damping originates from SOC of CoFeB film. However, when IMA becomes relatively small in Si/SiO_2/Ta/CoFeB/MgO films, its correlation with two-fold anisotropy is not experimentally observed. We believe that our work will help to design the orientational anisotropy in damping in future spintronics devices by engineering bulk and interfacial SOC strengths.

Methods

Sample fabrication. RF sputtering was used to deposit multilayer films Ta(10)/$Co_{20}Fe_{60}B_{20}$ (t = 1.6, 1.8, 2.0, 2.2)/MgO(2)/Al_2O_3(10) on Si/SiO_2(700) substrates and Ta(10)/$Co_{20}Fe_{60}B_{20}$(2.0)/MgO(2)/Al_2O_3(10) on Y-cut $LiNbO_3$ substrates at room temperature followed by vacuum annealing for 60 min at 280 °C temperature under 600 mT magnetic field applied along out-of-plane direction to the films. In the first step of fabrication, rectangular structures with lateral dimensions of $200 \times 12\ \mu m^2$ were defined on the deposited films with the help of maskless UV lithography followed by Ar^+ ion milling down to the substrate. End point mass detector was used during the ion milling to ensure the right time to stop ion milling. In the second step, metal gate contacts at the edges of rectangular structures for measuring inverse spin Hall (ISHE) signals were prepared with the help of UV lithography and followed by the deposition of Ti(5)/Au(100) layer by electron beam evaporation. In the following step, 180-nm-thick Al_2O_3 layer was deposited by RF magnetron sputtering everywhere except on top of the edges of metal contacts made for measuring ISHE signals. In the final step, the microwave antennae for the excitation of FMR were prepared by maskless UV lithography followed by the deposition of Ti(5)/Au(200) layer by electron beam evaporation. It should be noted here that the microwave antennae are electrically isolated from rectangular CoFeB strips by 180-nm-thick Al_2O_3 layer.

Experimental measurement. The FMR in CoFeB layers were excited by applying microwave current (i.e. I_{rf} (ω) from a signal generator) through the micrometer-sized antenna surrounding the rectangular shaped ($200 \times 12\ \mu m^2$) magnetic film. This RF current through the antenna generates a microwave magnetic field (h_{rf}) perpendicular to the film plane. The H is swept from − 320 mT to + 320 mT while keeping the frequency of RF current as fixed. At the resonance condition, a significantly large pure spin current (I_s) is pumped from CoFeB layer into the adjacent Ta buffer layer, where I_s is converted into a transverse charge current (I_c) through inverse spin Hall effect (ISHE) of Ta. The ISHE signal (V_{ISHE}) is then measured by a nanovoltmeter. To study angular dependent behavior of damping the measurements were repeated for various in-plane orientations of bias magnetic field at a step of 7.5° or 15° with respect to the long axis of the rectangular devices. In all the measurements the applied bias magnetic field was much larger than the IMA field, which rules out the increment of FMR linewidth as a consequence of field dragging effect.

Data availability

The datasets used and/or analysed during the current study available from the corresponding author on reasonable request.

Received: 28 February 2023; Accepted: 23 May 2023
Published online: 26 May 2023

Reference

1. Barman, A. & Sinha, J. *Spin Dynamics and Damping in Ferromagnetic Thin Films and Nanostructures* (Springer, 2018).
2. Safonov, V. L. Tensor form of magnetization damping. *J. Appl. Phys.* **91**, 8653–8655 (2002).
3. Seib, J., Steiauf, D. & Fähnle, M. Linewidth of ferromagnetic resonance for systems with anisotropic damping. *Phys. Rev. B* **79**, 092418 (2009).
4. Gilmore, K., Stiles, M. D., Seib, J., Steiauf, D. & Fähnle, M. Anisotropic damping of the magnetization dynamics in Ni Co, and Fe. *Phys. Rev. B* **81**, 174414 (2010).
5. Meckenstock, R., Spoddig, D., Frait, Z., Kambersky, V. & Pelzl, J. Anisotropic Gilbert damping in epitaxial Fe films on InAs(001). *J. Magn. Magn. Mater.* **272–276**, 1203–1204 (2004).
6. Zhai, Y. *et al.* A study on ferromagnetic resonance linewidth of single crystalline ultrathin Fe film grown on GaAs substrate. *J. Appl. Phys.* **101**, 09D120 (2007).
7. Kasatani, Y. & Nozaki, Y. Crystallographic anisotropy of the intrinsic Gilbert damping for single-crystalline Fe film. *J. Magn. Soc. Jpn.* **39**, 221–226 (2015).
8. Chen, L. *et al.* Emergence of anisotropic Gilbert damping in ultrathin Fe layers on GaAs(001). *Nat. Phys.* **14**, 490–494 (2018).
9. Li, Y. *et al.* Giant anisotropy of Gilbert damping in epitaxial CoFe films. *Phys. Rev. Lett.* **122**, 117203 (2019).
10. Thonig, D. & Henk, J. Gilbert damping tensor within the breathing Fermi surface model: Anisotropy and non-locality. *New J. Phys.* **16**, 013032 (2014).
11. Gilmore, K., Idzerda, Y. U. & Stiles, M. D. Identification of the dominant precession-damping mechanism in Fe Co, and Ni by first-principles calculations. *Phys. Rev. Lett.* **99**, 027204 (2007).
12. Brataas, A., Tserkovnyak, Y. & Bauer, G. E. W. Scattering theory of Gilbert damping. *Phys. Rev. Lett.* **101**, 037207 (2008).
13. Mankovsky, S., Ködderitzsch, D., Woltersdorf, G. & Ebert, H. First-principles calculation of the Gilbert damping parameter via the linear response formalism with application to magnetic transition metals and alloys. *Phys. Rev. B* **87**, 014430 (2013).
14. Barsukov, I. *et al.* Magnetocrystalline anisotropy and Gilbert damping in iron-rich $Fe_{1-x}Si_x$ thin films. *Phys. Rev. B* **84**, 180405 (2011).
15. Scheck, C., Cheng, L., Barsukov, I., Frait, Z. & Bailey, W. E. Low relaxation rate in epitaxial vanadium-doped ultrathin iron films. *Phys. Rev. Lett.* **98**, 117601 (2007).
16. Schoen, M. A. W. *et al.* Ultra-low magnetic damping of a metallic ferromagnet. *Nat. Phys.* **12**, 839–842 (2016).
17. Suhl, H. Theory of the magnetic damping constant. *IEEE Trans. Magn.* **34**, 1834–1838 (1998).
18. Ando, K. *et al.* Inverse spin-Hall effect induced by spin pumping in metallic system. *J. Appl. Phys.* **109**, 103913 (2011).
19. Shaw, J. M., Nembach, H. T. & Silva, T. J. Determination of spin pumping as a source of linewidth in sputtered Co90Fe10/Pd multilayers by use of broadband ferromagnetic resonance spectroscopy. *Phys. Rev. B* **85**, 054412 (2012).
20. Chen, K. & Zhang, S. Spin pumping in the presence of spin-orbit coupling. *Phys. Rev. Lett.* **114**, 126602 (2015).
21. Ganguly, A. *et al.* Time-domain detection of current controlled magnetization damping in Pt/Ni81Fe19 bilayer and determination of Pt spin Hall angle. *Appl. Phys. Lett.* **105**, 112409 (2014).
22. Rojas-Sánchez, J. C. *et al.* Spin pumping and inverse spin Hall effect in Platinum: the essential role of spin-memory loss at metallic interfaces. *Phys. Rev. Lett.* **112**, 106602 (2014).
23. Tao, X. *et al.* Self-consistent determination of spin Hall angle and spin diffusion length in Pt and Pd: The role of the interface spin loss. *Sci. Adv.* **4**, 1670 (2018).
24. Ament, W. S. & Rado, G. T. Electromagnetic effects of spin wave resonance in ferromagnetic metals. *Phys. Rev.* **97**, 1558–1566 (1955).
25. Schoen, M. A. W., Shaw, J. M., Nembach, H. T., Weiler, M. & Silva, T. J. Radiative damping in waveguide-based ferromagnetic resonance measured via analysis of perpendicular standing spin waves in sputtered permalloy films. *Phys. Rev. B* **92**, 184417 (2015).
26. Woltersdorf, G. & Heinrich, B. Two-magnon scattering in a self-assembled nanoscale network of misfit dislocations. *Phys. Rev. B* **69**, 184417 (2004).
27. Azevedo, A., Oliveira, A. B., de Aguiar, F. M. & Rezende, S. M. Extrinsic contributions to spin-wave damping and renormalization in thin $Ni_{50}Fe_{50}$ films. *Phys. Rev. B* **62**, 5331–5333 (2000).
28. Zhu, L., Zhu, L., Ralph, D. C. & Buhrman, R. A. Origin of strong two-magnon scattering in heavy-metal/ferromagnet/oxide heterostructures. *Phys. Rev. Applied* **13**, 034038 (2020).
29. Lindner, J. *et al.* Two-magnon damping in thin films in case of canted magnetization: Theory versus experiment. *Phys. Rev. B* **80**, 224421 (2009).
30. Lenz, K. *et al.* Two-magnon scattering and viscous Gilbert damping in ultrathin ferromagnets. *Phys. Rev. B* **73**, 144424 (2006).
31. McMichael, R. D., Stiles, M. D., Chen, P. J. & Egelhoff, W. F. Jr. Ferromagnetic resonance linewidth in thin films coupled to NiO. *J. Appl. Phys.* **83**, 7037–7039 (1998).
32. Mills, D. L. & Arias, R. The damping of spin motions in ultrathin films: Is the Landau–Lifschitz–Gilbert phenomenology applicable?. *Physica B* **384**, 147–151 (2006).
33. Conca, A., Keller, S., Schweizer, M. R., Papaioannou, E. T. & Hillebrands, B. Separation of the two-magnon scattering contribution to damping for the determination of the spin mixing conductance. *Phys. Rev. B* **98**, 214439 (2018).
34. Arias, R. & Mills, D. L. Extrinsic contributions to the ferromagnetic resonance response of ultrathin films. *Phys. Rev. B* **60**, 7395–7409 (1999).
35. Hellman, F. *et al.* Interface-induced phenomena in magnetism. *Rev. Mod. Phys.* **89**, 025006 (2017).
36. Rana, B., Fukuma, Y., Miura, K., Takahashi, H. & Otani, Y. Excitation of coherent propagating spin waves in ultrathin CoFeB film by voltage-controlled magnetic anisotropy. *Appl. Phys. Lett.* **111**, 052404 (2017).
37. Ikeda, S. *et al.* A perpendicular-anisotropy CoFeB–MgO magnetic tunnel junction. *Nat. Mater.* **9**, 721–724 (2010).
38. Mruczkiewicz, M. & Krawczyk, M. Influence of the Dzyaloshinskii-Moriya interaction on the FMR spectrum of magnonic crystals and confined structures. *Phys. Rev. B* **94**, 024434 (2016).
39. Puebla, J. *et al.* Direct optical observation of spin accumulation at nonmagnetic metal/oxide interface. *Appl. Phys. Lett.* **111**, 092402 (2017).
40. Lesne, E. *et al.* Highly efficient and tunable spin-to-charge conversion through Rashba coupling at oxide interfaces. *Nat. Mater.* **15**, 1261 (2016).
41. Azzawi, S. *et al.* Evolution of damping in ferromagnetic/nonmagnetic thin film bilayers as a function of nonmagnetic layer thickness. *Phys. Rev. B* **93**, 054402 (2016).

42. Pal, S., Rana, B., Hellwig, O., Thomson, T. & Barman, A. Tunable magnonic frequency and damping in [Co/Pd]$_8$ multilayers with variable Co layer thickness. *Appl. Phys. Lett.* **98**, 082501 (2011).
43. Enobio, E. C. I., Sato, H., Fukami, S., Matsukura, F. & Ohno, H. CoFeB thickness dependence of damping constants for single and double CoFeB-MgO interface structures. *IEEE Magn. Lett.* **6**, 1–3 (2015).
44. Okada, A. *et al.* Electric-field effects on magnetic anisotropy and damping constant in Ta/CoFeB/MgO investigated by ferromagnetic resonance. *Appl. Phys. Lett.* **105**, 052415 (2014).
45. Rana, B. *et al.* Nonlinear control of damping constant by electric field in ultrathin ferromagnetic films. *Phys. Rev. Appl.* **14**, 014037 (2020).
46. Rana, B., Miura, K., Takahashi, H. & Otani, Y. Underlayer material dependent symmetric and asymmetric behavior of voltage-controlled magnetic anisotropy in CoFeB films. *J. Phys. Condens. Matter* **32**, 414002 (2020).
47. Xu, M. *et al.* Nonreciprocal surface acoustic wave propagation via magneto-rotation coupling. *Sci. Adv.* **6**, 1724 (2020).
48. Liu, L., Moriyama, T., Ralph, D. C. & Buhrman, R. A. Spin-torque ferromagnetic resonance induced by the spin Hall effect. *Phys. Rev. Lett.* **106**, 036601 (2011).
49. Kondou, K., Sukegawa, H., Mitani, S., Tsukagoshi, K. & Kasai, S. Evaluation of spin Hall angle and spin diffusion length by using spin current-induced ferromagnetic resonance. *Appl. Phys. Express* **5**, 073002 (2012).
50. Rana, B. *et al.* Electric field control of spin waves in ultrathin CoFeB films. *Phys. Rev. B* **100**, 224412 (2019).
51. Deka, A. *et al.* Electric field induced parametric excitation of exchange magnons in a CoFeB/MgO junction. *Phys. Rev. Res.* **4**, 023139 (2022).
52. Deka, A. *et al.* Electric-field control of interfacial in-plane magnetic anisotropy in CoFeB/MgO junctions. *Phys. Rev. B* **101**, 174405 (2020).
53. Tserkovnyak, Y., Brataas, A., Bauer, G. E. W. & Halperin, B. I. Nonlocal magnetization dynamics in ferromagnetic heterostructures. *Rev. Mod. Phys.* **77**, 1375–1421 (2005).
54. Panda, S. N., Mondal, S., Sinha, J., Choudhury, S. & Barman, A. All-optical detection of interfacial spin transparency from spin pumping in β-Ta/CoFeB thin films. *Sci. Adv.* **5**, 7200 (2019).
55. Belmeguenai, M. *et al.* Co_2FeAl thin films grown on MgO substrates: Correlation between static, dynamic, and structural properties. *Phys. Rev. B* **87**, 184431 (2013).
56. Tu, H. *et al.* Large anisotropy of magnetic damping in amorphous CoFeB films on GaAs(001). *J. Phys. Condens. Matter* **32**, 335804 (2020).
57. Wang, Z. *et al.* Atomic-scale structure and local chemistry of CoFeB–MgO magnetic tunnel junctions. *Nano Lett.* **16**, 1530–1536 (2016).
58. Waseda, Y., Hirata, K. & Ohtani, M. High-temperature thermal expansion of platinum, tantalum, molybdenum, and tungsten measured by X-ray diffraction. *High Temp. High Pressures* **7**, 221–226 (1975).
59. Rezende, S. M., Azevedo, A., Lucena, M. A. & de Aguiar, F. M. Anomalous spin-wave damping in exchange-biased films. *Phys. Rev. B* **63**, 214418 (2001).
60. Beik Mohammadi, J. *et al.* Broadband ferromagnetic resonance characterization of anisotropies and relaxation in exchange-biased IrMn/CoFe bilayers. *Phys. Rev. B* **95**, 064414 (2017).
61. Zakeri, K. *et al.* Spin dynamics in ferromagnets: Gilbert damping and two-magnon scattering. *Phys. Rev. B* **76**, 104416 (2007).
62. Barsukov, I. *et al.* Tuning magnetic relaxation by oblique deposition. *Phys. Rev. B* **85**, 014420 (2012).

Acknowledgements
BR acknowledges RIKEN Incentive Research Project with grant number FY2019, Adam Mickiewicz University for "Initiative of Excellence - Research University" (ID-UB) project with grant number 038/04/NŚ/0037, and the NCN SONATA-16 project with Grant Number 2020/39/D/ST3/02378. The authors sincerely thank Dr. Katsuya Miura and Dr. Hiromasa Takahashi from the Research and Development Group, Hitachi Ltd., Tokyo, Japan, for preparing the thin films for the study.

Author contributions
B.R. fabricated the devices, performed measurements, analyzed data. Both authors discussed the results and wrote manuscript.

Competing interests
The authors declare no competing interests.

Additional information
Supplementary Information The online version contains supplementary material available at https://doi.org/10.1038/s41598-023-35739-8.

Correspondence and requests for materials should be addressed to B.R.